

# Effect of Mg<sup>2+</sup> and Na<sup>+</sup> on the Nucleic Acid Chaperone Activity of HIV-1 Nucleocapsid Protein: Implications for Reverse Transcription

My-Nuong Vo<sup>1</sup>, George Barany<sup>1</sup>, Ioulia Rouzina<sup>2\*</sup>  
and Karin Musier-Forsyth<sup>3\*</sup>

<sup>1</sup>Department of Chemistry and  
Institute for Molecular Virology,  
University of Minnesota,  
Minneapolis, MN 55455, USA

<sup>2</sup>Department of Biochemistry,  
Molecular Biology and  
Biophysics, University of  
Minnesota, Minneapolis,  
MN 55455, USA

<sup>3</sup>Departments of Chemistry  
and Biochemistry, The Ohio  
State University, Columbus,  
OH 43210, USA

Received 30 August 2008;  
received in revised form  
20 December 2008;  
accepted 29 December 2008  
Available online  
6 January 2009

The human immunodeficiency virus type 1 (HIV-1) nucleocapsid protein (NC) is an essential protein for retroviral replication. Among its numerous functions, NC is a nucleic acid (NA) chaperone protein that catalyzes NA rearrangements leading to the formation of thermodynamically more stable conformations. *In vitro*, NC chaperone activity is typically assayed under conditions of low or no Mg<sup>2+</sup>, even though reverse transcription requires the presence of divalent cations. Here, the chaperone activity of HIV-1 NC was studied as a function of varying Na<sup>+</sup> and Mg<sup>2+</sup> concentrations by investigating the annealing of complementary DNA and RNA hairpins derived from the *trans*-activation response domain of the HIV genome. This reaction mimics the annealing step of the minus-strand transfer process in reverse transcription. Gel-shift annealing and sedimentation assays were used to monitor the annealing kinetics and aggregation activity of NC, respectively. In the absence of protein, a limited ability of Na<sup>+</sup> and Mg<sup>2+</sup> cations to facilitate hairpin annealing was observed, whereas NC stimulated the annealing 10<sup>3</sup>- to 10<sup>5</sup>-fold. The major effect of either NC or the cations is on the rate of bimolecular association of the hairpins. This effect is especially strong under conditions wherein NC induces NA aggregation. Titration with NC and NC/Mg<sup>2+</sup> competition studies showed that the annealing kinetics depends only on the level of NA saturation with NC. NC competes with Mg<sup>2+</sup> or Na<sup>+</sup> for sequence-nonspecific NA binding similar to a simple trivalent cation. Upon saturation, NC induces attraction between NA molecules corresponding to ~0.3 kcal/mol/nucleotide, in agreement with an electrostatic mechanism of NC-induced NA aggregation. These data provide insights into the variable effects of NC's chaperone activity observed during *in vitro* studies of divalent metal-dependent reverse transcription reactions and suggest the feasibility of NC-facilitated proviral DNA synthesis within the mature capsid core.

© 2009 Elsevier Ltd. All rights reserved.

**Keywords:** nucleic acid chaperone activity; HIV-1 nucleocapsid protein; nucleic acid aggregation; multivalent cations; electrostatics of nucleic acids

Edited by J. Doudna

\*Corresponding authors. E-mail addresses: rouzi002@umn.edu; musier@chemistry.ohio-state.edu.

Present address: M.-N. Vo, The Scripps Research Institute, 10550 North Torrey Pines Road, La Jolla, CA 92037, USA.

Abbreviations used: TAR, *trans*-activation response element; NC, nucleocapsid protein; NA, nucleic acid; HIV-1, human immunodeficiency virus type 1; RT, reverse transcriptase.

## Introduction

Human immunodeficiency virus type 1 (HIV-1) nucleocapsid protein (NC) is a highly cationic 55-amino-acid protein derived upon proteolysis of the Gag and Gag-Pol polyprotein precursors.<sup>1–3</sup> Like most other retroviral NC proteins, HIV-1 NC, or the NC domain of Gag, is known to play a role in packaging viral RNA<sup>4,5</sup> or nonviral RNA,<sup>6–8</sup> virus assembly,<sup>9–12</sup> viral RNA dimerization<sup>13,14</sup> and maturation,<sup>15,16</sup> tRNA primer annealing to the viral RNA template,<sup>14,17–20</sup> reverse transcription,<sup>21</sup> and integration.<sup>22–24</sup> Many of these functions of NC are a result of its so-called general nucleic acid (NA) chaperone activity.<sup>21,25–27</sup> This property of HIV NC relies on its ability to bind to a diverse array of NA sequences with comparable affinity,<sup>27–33</sup> allowing it to chaperone a wide variety of NA annealing and remodeling reactions leading to structures with maximal stability.

*In vitro* studies have shown that optimal NA chaperone activity requires saturated protein binding corresponding to 1 NC molecule per 6 ± 1 nt.<sup>29,30,32–36</sup> Upon saturation with NC, NA secondary structures are moderately destabilized.<sup>37–46</sup> Wild-type HIV-1 NC also possesses potent NA aggregating activity.<sup>25,27,47–49</sup> Whereas the duplex destabilizing activity of NC has been mapped to its zinc finger domains,<sup>39,50–53</sup> the ability to aggregate NA is largely due to NC's highly cationic N-terminal domain.<sup>33,41,48,49,54</sup> Recently, the fast kinetics of NC dissociation from both single-stranded and double-stranded NA was shown to be another key characteristic of HIV-1 NC's chaperone activity.<sup>54,55</sup>

The effect of NC on the kinetics of annealing complementary NA<sup>18,27,29,34,36,50,56–58</sup> and on various steps of reverse transcription<sup>21,50,59–64</sup> has been extensively studied *in vitro*. In all these studies, although stimulation by NC was detected, the magnitude of this effect varied. For example, in studies focusing on annealing of complementary oligonucleotides, the overall rate enhancement measured in the presence of wild-type HIV-1 NC ranged from 10- to 10<sup>5</sup>-fold.<sup>18,29,34,36,58</sup> One explanation of the variable effect of NC is the wide variety of substrates used in these studies. In a systematic study of NC's chaperone function, the rate of annealing of complementary NA of lower initial stability was shown to be stimulated much less by NC than for substrates with high initial stability.<sup>65</sup> In addition, if the starting structures are too stable, NC's relatively moderate destabilizing activity is unable to facilitate duplex unwinding and annealing.<sup>18,37,38,66</sup> A major factor in NC's ability to stimulate the annealing of highly structured substrates has been attributed to its ability to aggregate NA molecules upon saturated binding.<sup>18,58</sup> In contrast, subsaturating levels of NC are sufficient for NA destabilization activity but generally lead to much weaker stimulation of annealing.<sup>37,38,40,58</sup> These results are consistent with studies using [NC(12–55)], which lacks the cationic N-terminal "aggregation domain".<sup>44,52,67</sup> In general, this truncated

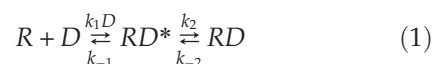
NC variant only stimulates annealing by ~10- to 100-fold.

NC has also been demonstrated to stimulate *in vitro* strand transfer reactions that mimic both the annealing and subsequent reverse transcriptase (RT) extension steps. These more complex reactions are monitored by observing the RT extension products on a gel. Interestingly, the effects of NC on stimulation of the complete strand transfer reaction are generally much less (~2- to 3-fold) than the effect observed in simple annealing assays.<sup>50,63,64,68–70</sup> A common feature of these assays is the presence of 6–10 mM Mg<sup>2+</sup> used in order to optimize RT activity. A recent study has shown that much lower Mg<sup>2+</sup> is sufficient to support RT activity<sup>71</sup> and is more relevant to *in vivo* conditions in most cell types. We hypothesize that the presence of high Mg<sup>2+</sup> concentrations in these strand transfer reactions leads to subsaturating levels of NC binding, thereby leading to minimal effects of NC on the overall strand transfer process. This hypothesis is qualitatively supported by the recent observation that higher Mg<sup>2+</sup> suppresses the effect of NC on *in vitro* strand transfer reactions.<sup>70</sup>

In this work, we test this hypothesis by performing a systematic study of the effect of Na<sup>+</sup> and Mg<sup>2+</sup> ions on NC-stimulated annealing of complementary RNA and DNA hairpins derived from the *trans*-activation response element (TAR) of the HIV genome. Gel-shift assays were used to monitor the kinetics of hairpin annealing over a broad range of NC concentrations, including conditions resulting in NA aggregation. A simple sedimentation assay was used to monitor fractional NA aggregation induced by NC. Taken together, these data help to explain the variable effects of NC's chaperone activity in stimulation of Mg<sup>2+</sup>-dependent strand transfer reactions and emphasize the importance of NA saturation with NC for optimal chaperone function *in vitro*.

## Results and Discussion

The TAR RNA and DNA substrates used in this work are shown in Fig. 1. Both full-length and truncated mini-TAR substrates (Fig. 1, boxed) were studied. The two-step annealing process can be described by the following reaction:



The first bimolecular step leads to the formation of RD\*, characterized by the forward association rate constant  $k_1$  and the intermediate dissociation rate  $k_{-1}$ . RD\* is subsequently converted into the fully annealed RNA/DNA duplex, RD, via the second monomolecular step, which is characterized by the strand-exchange rate  $k_2$  and reverse rate  $k_{-2}$ .

Under the majority of solution conditions studied in this work, the TAR RNA/DNA annealing kinetics is biexponential. The percentage of molecules

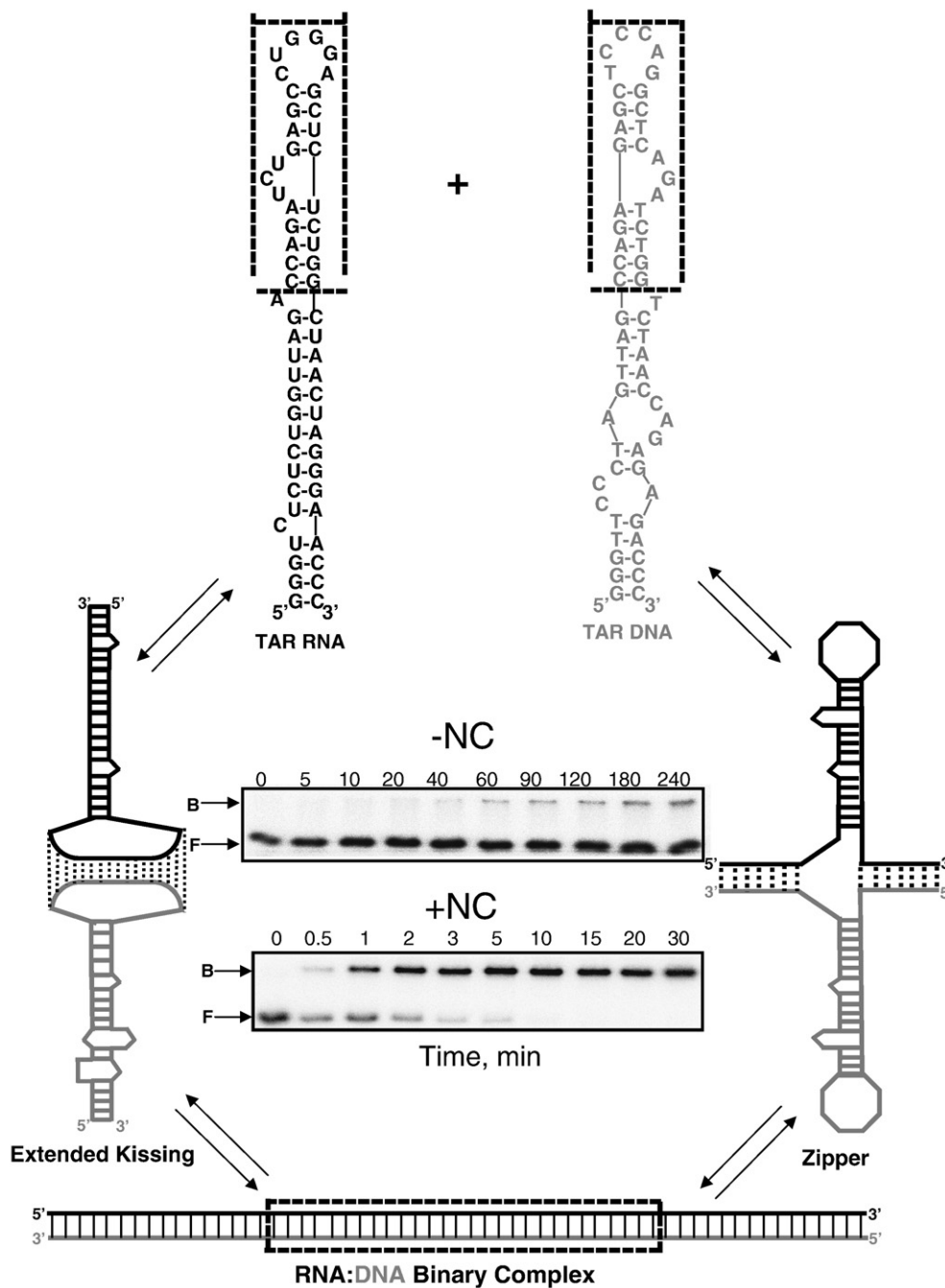


**Fig. 1.** Multiple pathways of TAR RNA/DNA annealing. Predicted secondary structures of full-length and mini-TAR RNA (black) and DNA (gray) hairpins are shown at the top. Sequences are derived from the HIV-1 NL4-3 isolate, and secondary structures were predicted by *m*-fold analysis.<sup>111</sup> The mini-TAR constructs are derived from the top part of each hairpin (dotted box). In the absence of NC, mini-TAR and full-length TAR RNA/DNA annealing involve initial formation of an extended loop-loop kissing interaction (middle, left) followed by strand exchange to form the fully annealed duplex (bottom). In the presence of saturating amounts of NC, full-length TAR RNA/DNA annealing involves nucleation through the 3'/5' termini resulting in the formation of a "zipper" intermediate (middle, right) prior to conversion to the fully annealed product.<sup>58,77</sup> Typical gels used to measure the TAR RNA/DNA annealing reaction time course in the absence (top) and presence (bottom) of saturating amounts of NC are also shown. The gel lanes are labeled with the reaction time in minutes. The bands corresponding to the bound and the free RNA are labeled B and F, respectively.

annealed as a function of time,  $P(t)$ , can be described as:

$$P(t) = P_{\infty} \cdot (f \cdot (1 - e^{-k_f t}) + (1 - f) \cdot (1 - e^{-k_s t})). \quad (2)$$

Here, the fast and the slow rates of annealing,  $k_f$  and  $k_s$ , correspond to the rate of formation of  $RD^*$  and  $RD$ , respectively, while  $f$  is the probability of intermediate formation and  $P_{\infty}$  is the final equilibrium percentage of RNA annealed. The following

equations describe the relationship between these kinetic parameters [Eq. (2)] and the elementary rates of the two-step process [Eq. (1)]:<sup>72</sup>

$$k_f = k_1 D + k_{-1} \quad \text{and} \quad k_s = f \cdot k_2 + k_{-2}, \quad (3)$$

where

$$f = \frac{k_1 D}{k_1 D + k_{-1}} = \frac{D/K_d^*}{D/K_d^* + 1} \quad \text{and} \\ P_\infty = 100 \cdot f \cdot \frac{k_2}{k_2 + k_{-2}} = 100 \cdot \frac{D/K_d}{D/K_d + 1} \quad (4)$$

Here,  $K_d^*$  and  $K_d$  are the equilibrium dissociation constants of  $RD^*$  and  $RD$ , respectively. Experimentally, both fast and slow rates are observed when they are sufficiently different from each other, that is,  $k_f \gg k_s$ , and when the partially annealed complex

has an intermediate stability, that is,  $0.1 < f < 0.9$ . If  $RD^*$  is very stable or very unstable, then only the fast or the slow rate can be determined, respectively. According to Eqs. (3) and (4), the fitted parameters  $k_f$ ,  $k_s$ , and  $f$  can be used to estimate the elementary rates of the two-step annealing process as:

$$k_1 = k_f \cdot \frac{f}{D}, \quad k_{-1} = k_f \cdot (1 - f), \\ k_2 = k_s / f, \quad K_d^* = \frac{k_{-1}}{k_1} = \frac{1 - f}{f} \cdot D \quad (5)$$

### Hairpin annealing kinetics in the absence of NC

To understand the effects of monovalent and divalent cations on the NA chaperone activity of HIV-1 NC, we first examined the annealing kinetics

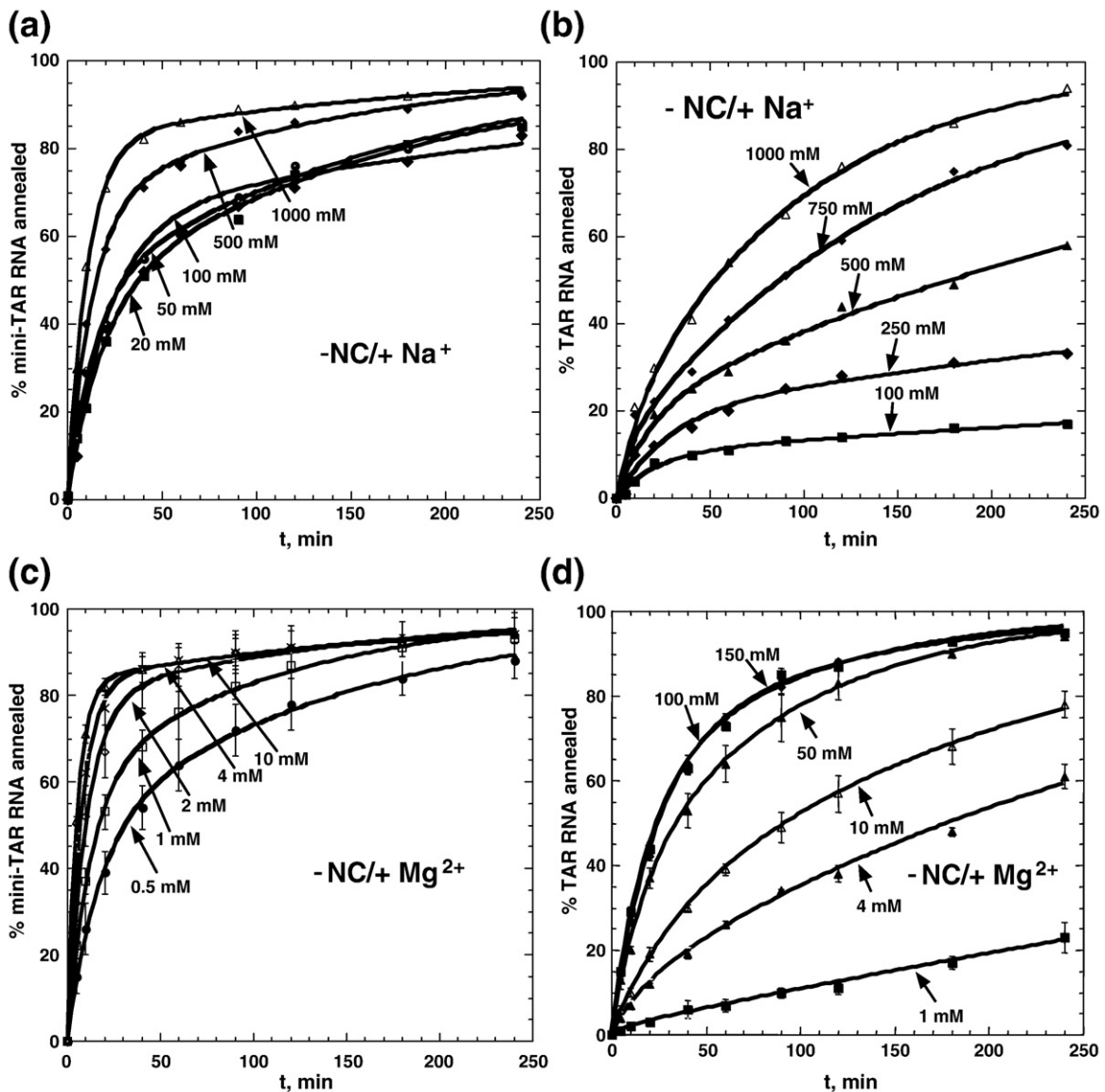


**Fig. 2.**  $Na^+$  and  $Mg^{2+}$  dependence of mini-TAR and full-length TAR RNA/DNA annealing in the absence of NC. Percentage of mini-TAR (a and c) or full-length TAR (b and d) RNA (15 nM) annealed to complementary DNA (300 nM) as a function of time at 37 °C in the presence of various concentrations of NaCl and  $MgCl_2$ , as indicated on each curve. Lines represent two-exponential fits of the data to Eq. (2), with the equilibrium percent annealed fixed at 100%.

of mini-TAR and full-length TAR hairpins (Fig. 1) as a function of  $Na^+$  and  $Mg^{2+}$  concentration in the absence of NC. As shown in Fig. 2a and b,  $Na^+$  ions facilitate hairpin annealing, with annealing of the shorter hairpins (Fig. 2a and c) stimulated at much lower salt than the longer TAR substrates (Fig. 2b and d).  $Mg^{2+}$  also facilitates hairpin annealing; however,  $\sim 10$ - to  $100$ -fold lower  $Mg^{2+}$  is sufficient to achieve the same effect as with  $Na^+$  (Fig. 2c and d).

#### Dependence of intermediate association rate on $Na^+$ and $Mg^{2+}$

To quantitatively determine the effect of cations on the annealing kinetics, we fit the annealing time courses in Fig. 2 to Eq. (2) with  $P_{\infty} = 100\%$  (i.e., the annealing of either mini-TAR or TAR is irreversible

in the absence of NC) to obtain  $k_s$ ,  $k_t$ , and  $f$ . The dissociation constant of the intermediate and the elementary reaction rates of the two-step annealing reaction were obtained using Eq. (5) and plotted in Fig. 3 as a function of  $Na^+$  and  $Mg^{2+}$  concentration. As shown in Fig. 3a, the bimolecular association rate,  $k_1$ , is  $\sim 10$ -fold faster for the shorter hairpins with both  $Na^+$  and  $Mg^{2+}$ . The fact that this difference between mini-TAR and full-length TAR hairpins does not disappear in higher salt suggests that the difference is not due to the stronger electrostatic repulsion between the longer molecules. Shubsda *et al.* also observed slower association of longer hairpins and attributed this difference to the larger entropy loss upon complex formation.<sup>73</sup>

Upon increasing  $[Na^+]$  from 20 to 1000 mM or  $[Mg^{2+}]$  from 0.2 to 150 mM,  $k_1$  increases from  $10^3$  to

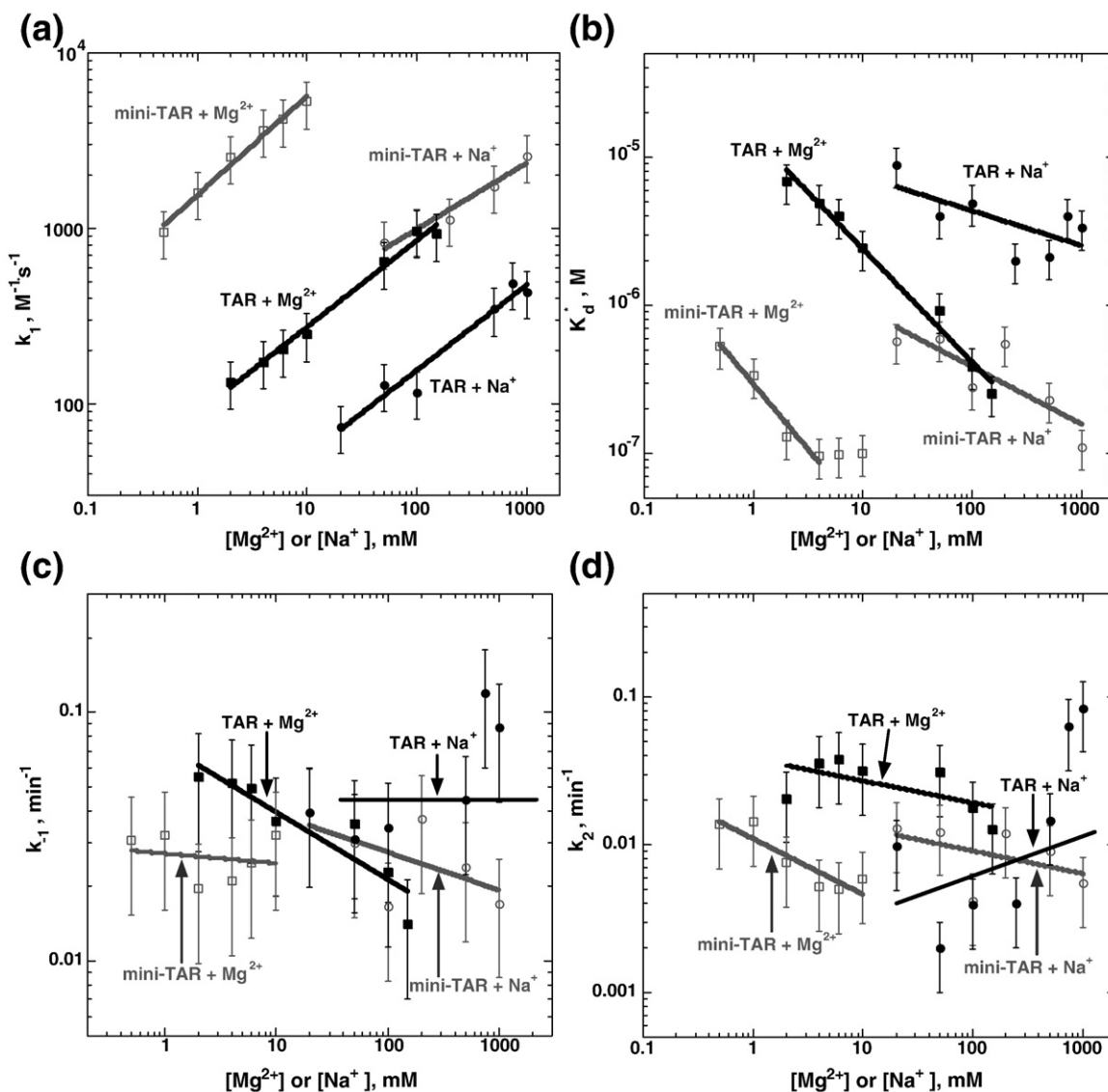


**Fig. 3.** Dependence of the intermediate dissociation constant and elementary rates of mini-TAR or full-length TAR RNA/DNA annealing on  $Na^+$  and  $Mg^{2+}$  in the absence of NC. (a) Intermediate association rate  $k_1$ , (b) dissociation constant  $K_d^*$ , (c) dissociation rate  $k_{-1}$ , and (d) strand-exchange rate  $k_2$  as a function of  $Na^+$  and  $Mg^{2+}$  concentration. The elementary reaction rates are obtained based on the data shown in Fig. 2. Gray and black lines represent mini-TAR and full-length TAR RNA/DNA annealing, respectively.

$10^4 \text{ M}^{-1} \text{ s}^{-1}$  for mini-TAR and from  $10^2$  to  $10^3 \text{ M}^{-1} \text{ s}^{-1}$  for full-length TAR hairpins. A further increase in the salt concentration does not lead to faster annealing. Consistent with these observations, the rates measured here are significantly slower than the typical association rates of unstructured complementary NA molecules, which are typically  $10^5$ – $10^6 \text{ M}^{-1} \text{ s}^{-1}$  under similar salt conditions.<sup>72,74–76</sup> As shown previously,  $k_1$  is stimulated by temperature for mini-TAR,<sup>58</sup> suggesting that  $k_1$  involves melting some part of the initial hairpin secondary structure to provide enough base-pairing interactions to nucleate stable intermediate formation. Mutational analysis of mini-TAR<sup>58</sup> and full-length TAR RNA/DNA<sup>77</sup> shows that in the absence of NC, annealing proceeds through the formation of an extended loop–loop intermediate (see Fig. 1, lower left).

As shown in Fig. 3a, the salt dependence of  $k_1$  is similar for mini-TAR and TAR hairpins. In general, the salt dependence of the rate or equilibrium constant of a process may be characterized by the following equation:<sup>78</sup>

$$s = \frac{d \log k}{d \log M} \quad (6)$$

Here,  $k$  is the rate,  $M$  is the cation concentration, and  $s$  corresponds to the number of cations associating (if  $s > 0$ ) or dissociating (if  $s < 0$ ) from the system during the process. For the association process characterized by rate  $k_1$ , the values of  $s$  were calculated from the slope of a plot of  $k_1$  versus  $[Na^+]$  or  $[Mg^{2+}]$  for both TAR hairpins. For mini-TAR,  $s = 0.4 \pm 0.1$  ( $Na^+$ ) and  $s = 0.6 \pm 0.1$  ( $Mg^{2+}$ ), whereas for full-length TAR,  $s = 0.6 \pm 0.1$  ( $Na^+$ ) and  $s = 0.5 \pm 0.1$  ( $Mg^{2+}$ ). These values are similar to the expected  $[Na^+]$  dependence for association rates of short complementary oligonucleotides.<sup>75</sup> These results are also consistent with a single-molecule fluorescence resonance energy transfer study, wherein a similar  $s$  value was measured by studying the  $[Mg^{2+}]$  dependence of the docking rate of the hairpin ribozyme.<sup>79</sup>

#### Dependence of intermediate dissociation rate on $Na^+$ and $Mg^{2+}$

The dissociation rate,  $k_{-1}$ , of the extended 17-bp kissing complex (Fig. 1, left) is similar for the mini-TAR and full-length TAR hairpins and is only weakly dependent on  $Na^+$  and  $Mg^{2+}$  concentration (Fig. 3c). This result is consistent with the formation of a similar intermediate for both short and long DNA/RNA hairpins. Indeed, the average value of  $k_{-1}$  ( $\sim 0.03 \text{ min}^{-1}$ ) is consistent with the expected dissociation rate of a 17-bp duplex at  $37^\circ \text{C}$ <sup>72</sup> and with the fact that in a transition state for NA strand dissociation, the two strands are still close together with most of the cations still associated.<sup>80</sup>

#### Dependence of the intermediate dissociation constant on $Na^+$ and $Mg^{2+}$

The extended kissing complex dissociation constant,  $K_d^*$ , decreases (i.e., the complex stability inc-

reases) with increasing  $Na^+$  or  $Mg^{2+}$  concentration (Fig. 3b). The stabilizing effects of  $Na^+$  and  $Mg^{2+}$  are comparable; however,  $\sim 100$ - to  $1000$ -fold higher  $[Na^+]$  is required relative to  $[Mg^{2+}]$ . The bimolecular complex stability (and the annealing kinetics in general; see Fig. 2c and d) saturates at  $[Mg^{2+}] \geq 3 \text{ mM}$  for the mini-TAR hairpins and at  $[Mg^{2+}] \geq 100 \text{ mM}$  for the full-length TAR hairpins. For both the short and long hairpins,  $\geq 1000 \text{ mM } Na^+$  is required to achieve maximal stability. The stability of the extended kissing complex between the shorter mini-TAR hairpins is  $\sim 10$ - to  $50$ -fold higher than that of the longer full-length TAR hairpins under all salt concentrations.

Both monovalent and divalent cations are likely to stabilize the reaction intermediate by facilitating its association rate.<sup>72,75,81</sup> Based on the  $[Na^+]$  dependence, an  $s$  value of  $-0.3 \pm 0.06$  was calculated for both the mini-TAR and full-length TAR complexes, further supporting the similar nature of the annealing intermediates. The  $K_d^*$  dependence on  $Mg^{2+}$  is stronger than that on  $Na^+$ , with  $s = -0.8 \pm 0.1$  for both the mini-TAR and full-length TAR hairpins (see Fig. 3b). This suggests that up to one additional  $Mg^{2+}$  associates with the extended kissing complexes upon intermediate formation. It is possible that this effect is associated with stronger stabilization of interhelical stacking by  $Mg^{2+}$ , as observed in the crystal structure of a hairpin kissing complex.<sup>82</sup> Between two and three  $Mg^{2+}$  cations were also shown to associate with the stacked kissing complex of hairpin constructs based on the RNA I/RNA II system.<sup>83,84</sup> We hypothesize that the relatively strong  $Mg^{2+}$  dependence of complex stability is associated with specific  $Mg^{2+}$  binding, since non-specific binding is expected to have a very weak ( $s \sim -0.1$ )  $Mg^{2+}$  dependence.<sup>80,81,85,86</sup> Similar results were reported for stabilization of the kissing complex formed by HIV-1 dimerization initiation signal hairpins in the presence of either  $\sim 1 \text{ mM } Mg^{2+}$  or  $\sim 2 \text{ M } Na^+$ .<sup>87</sup> However, in contrast to our results and in agreement with data for polymeric DNA,<sup>72,88</sup> a stronger dependence of kissing complex stability on  $Na^+$  than on  $Mg^{2+}$  was observed.<sup>87</sup> The latter may be related to efficient coaxial stacking of the two hairpin duplexes in the kissing complex, making it more similar to polymeric DNA.

The observed 10- to 50-fold higher stability of the intermediate complex formed by the shorter hairpins appears to be nonelectrostatic in origin, since it does not disappear at higher salt. This stability difference is almost entirely due to a faster association rate for the shorter hairpins because the dissociation rate is  $< 2$ -fold slower than that for full-length TAR (see Fig. 3c). Therefore, the higher stability of the mini-TAR complex is likely due to a lower cost associated with the reduction in conformational freedom upon kissing complex formation.<sup>89</sup>

#### Dependence of the strand-exchange rate on $Na^+$ and $Mg^{2+}$

Figure 3d shows the  $Na^+$  and  $Mg^{2+}$  dependence on the strand-exchange rate,  $k_2$ . Although slightly

more pronounced than that for  $k_{-1}$ , the salt dependence of  $k_2$  is still very weak, and the rate is reduced in high salt with  $s = -0.25 \pm 0.1$ . The average value of  $k_2$  over the salt range studied for both TAR systems is  $\sim 0.01 \text{ min}^{-1}$ , which is about 3-fold slower than that of  $k_{-1}$ . This suggests that the first step of the formation of  $RD^*$  is in pre-equilibrium to the subsequent strand-exchange step. Surprisingly, the strand-exchange rate for the longer hairpins is practically indistinguishable within experimental accuracy from that of the shorter hairpins. This result suggests that the strand exchange is rate-limited not by opening of the base pairs along the hairpin stem but by a conformational change, most likely involving cooperative melting of a large fragment of one or both hairpin stems. This hypothesis is in agreement with the fact that the strand-exchange rate for four-way junction migration is much faster than the  $k_2$  measured here.<sup>90–93</sup>

### NC effect on the kinetics of mini-TAR and full-length TAR DNA/RNA annealing

#### Effect of NC concentration on mini-TAR and full-length TAR RNA/DNA annealing in low salt

Presented in Fig. 4 are typical annealing time courses for mini-TAR (a) and full-length TAR (b) hairpins in 20 mM NaCl. Under these low salt conditions, all NC added is expected to be bound to NA. These time courses were fit to Eq. (2) to obtain  $k_f$ ,  $k_s$ , and  $f$ , as well as the elementary rates according to Eq. (5). The reaction rates,  $k_1$ ,  $k_{-1}$ , and  $k_2$ , as well as  $K_d^*$ , are presented in Fig. 6 as a function of fractional saturation of NA with NC,  $\Theta_{NC}$  (see below). While the two-step mechanism of annealing persists as the NAs become saturated with NC, the annealing pathway changes, as described previously for both mini-TAR and TAR.<sup>58,77</sup>

The annealing kinetics was also examined under varying NC/ $Mg^{2+}$  solution conditions. Presented in Fig. 5 are the annealing time courses of mini-TAR and full-length TAR hairpins measured with two different titration procedures. In Fig. 5a (mini-TAR) and b (TAR),  $Mg^{2+}$  concentration was held constant at 1 mM and NC was varied from 2 to 20  $\mu\text{M}$ . As expected, in both cases, the annealing of the hairpins was more effectively facilitated by higher NC concentration. Figure 5c (mini-TAR) and d (TAR) present the results of a study wherein NC concentration was held constant at 5  $\mu\text{M}$  and  $Mg^{2+}$  was varied from 0.5 to 5 mM. Increasing  $Mg^{2+}$  slows down the annealing kinetics, with a more dramatic effect on the TAR hairpins. We hypothesize that  $Mg^{2+}$  competes with NC for binding to the NA substrates, thereby decreasing the catalytic effect of NC on hairpin annealing. Thus, the dissociation constant of NC,  $K_d^{NC}(\text{Mg})$ , increases with increasing  $[Mg^{2+}]$  and the concentrations of NC that result in similar fractional NC binding,  $\Theta_{NC} \sim [\text{NC}]/K_d^{NC}(\text{Mg})$ , should lead to the same reaction kinetics. In the absence of  $Mg^{2+}$ , under the low salt conditions used here,  $\Theta_{NC}$  is determined simply by the amount of added NC:

$$\Theta_{NC} = (\text{NC} : \text{nt}) \times 6 \quad (7)$$

Here, saturated binding (i.e.,  $\Theta_{NC} = 1$ ) was assumed to be achieved at a value of 1 NC per  $6 \pm 1$  nt.<sup>29,33–36,94</sup>

#### Comparison of NC's effect on the elementary rates of hairpin annealing with and without $Mg^{2+}$

In Fig. 6, the elementary reaction rates ( $k_1$ ,  $k_{-1}$ , and  $k_2$ ) and  $K_d^*$  for mini-TAR and TAR are presented as a function of  $\Theta_{NC}$ . The reaction rates were determined based on the data shown in Figs. 4 and 5. For experiments performed under low salt solution

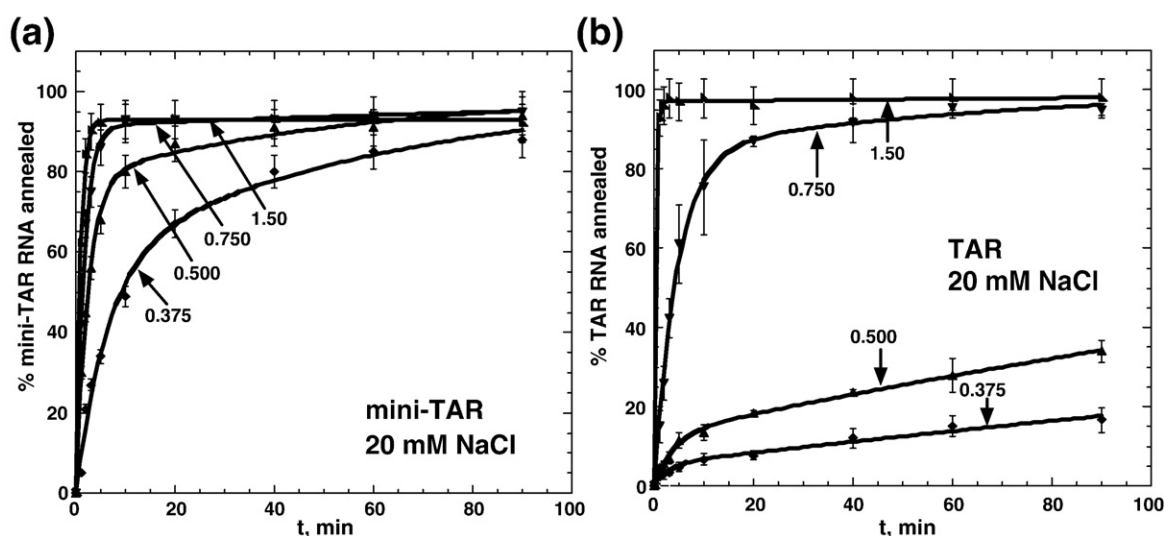


**Fig. 4.** NC concentration dependence of mini-TAR and full-length TAR RNA/DNA annealing in low salt. Percentage of mini-TAR (a) or full-length TAR (b) RNA (15 nM) annealed to 150 nM complementary DNA as a function of time in the presence of various concentrations of NC in 20 mM NaCl and 0.2 mM  $MgCl_2$ . Numbers indicate the fractional NC binding,  $\Theta_{NC}$ , as defined according to Eq. (2). Lines represent two-exponential fits of the data.

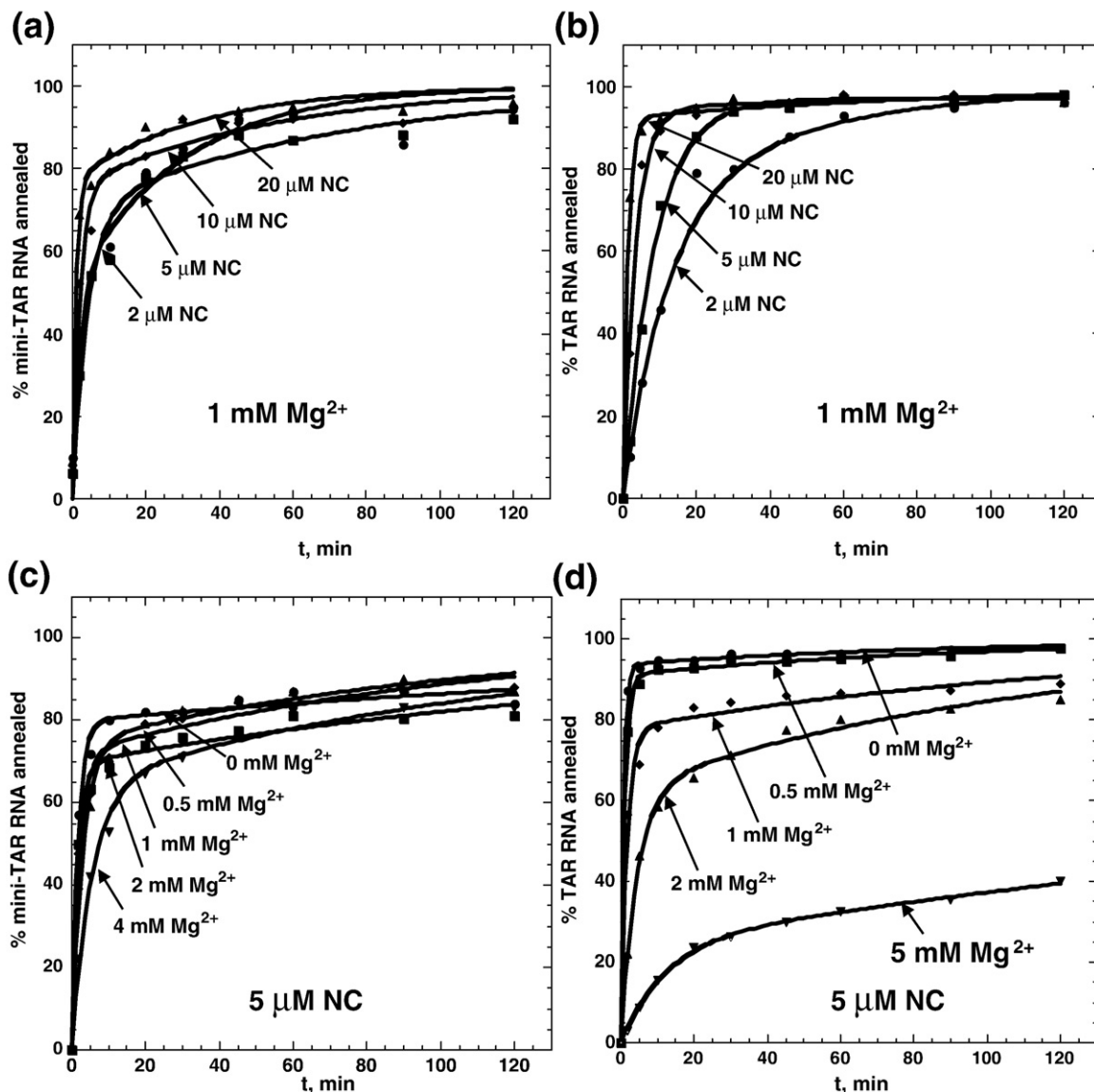


**Fig. 5.**  $Mg^{2+}$  dependence of NC-facilitated mini-TAR and full-length TAR RNA/DNA annealing. Percentage of mini-TAR (a) or full-length TAR (b) RNA (15 nM) annealed to complementary DNA (90 nM) as a function of time with 1 mM  $MgCl_2$  in the presence of various concentrations of NC, as indicated on each curve. Percentage of mini-TAR (c) or full-length TAR (d) RNA (15 nM) annealed to 90 nM complementary DNA as a function of time with 5  $\mu M$  NC in the presence of various concentrations of  $MgCl_2$ , as indicated on each curve. Lines represent two-exponential fits of the data.

( $[Mg^{2+}] = 0.2$  mM,  $[Na] = 20$  mM),  $\Theta_{NC}$  was determined according to Eq. (7). For  $Mg^{2+}/NC$  competition assays,  $\Theta_{NC}$  was estimated for each set of NC and  $Mg^{2+}$  concentrations assuming nonspecific electrostatic binding of NC and  $Mg^{2+}$  [see Eqs. (A1) and (A2) in the Supplementary Material]. The data from three independent series of experiments are plotted in the graphs shown in Fig. 6. A similar dependence of all rates on  $\Theta_{NC}$  is observed, supporting the hypothesis that nonspecific electrostatic NC/ $Mg^{2+}$  competition controls NC's binding and annealing kinetics.

#### Effect of NC on intermediate association rate

The effect of NC on  $k_1$  is very strong (Fig. 6a). In all three sets of experiments, the major change in  $k_1$

occurs within the range of  $0.2 < \Theta_{NC} < 0.5$  and  $0.5 < \Theta_{NC} < 1$  for mini-TAR and TAR RNA/DNA, respectively. In addition, the effect of NC saturation on  $k_1$  for the longer TAR hairpins is significantly greater than that for the shorter mini-TAR hairpins. In particular,  $k_1$  for the mini-TAR hairpins increases from  $\sim 10^2$   $M^{-1} s^{-1}$  in the absence of NC to  $\sim 10^5$   $M^{-1} s^{-1}$  at saturated NC, while this variation of  $k_1$  is between  $\sim 10$   $M^{-1} s^{-1}$  and  $\sim 4 \times 10^5$   $M^{-1} s^{-1}$  for the TAR hairpins. While  $\sim 1$  M  $Na^+$  or  $\sim 10$  mM  $Mg^{2+}$  is required for maximal  $k_1$  facilitation in the absence of NC (Fig. 3a), only  $\sim 1$   $\mu M$  NC is sufficient in the absence of  $Mg^{2+}$ . In the case of  $Mg^{2+}$  or  $Na^+$ ,  $k_1$  facilitation is a result of better screening of NA charge by these cations. However,  $k_1$  also involves premelting of the upper stem of the hairpins, which is probably slightly inhibited by  $Mg^{2+}$  and  $Na^+$ . As a

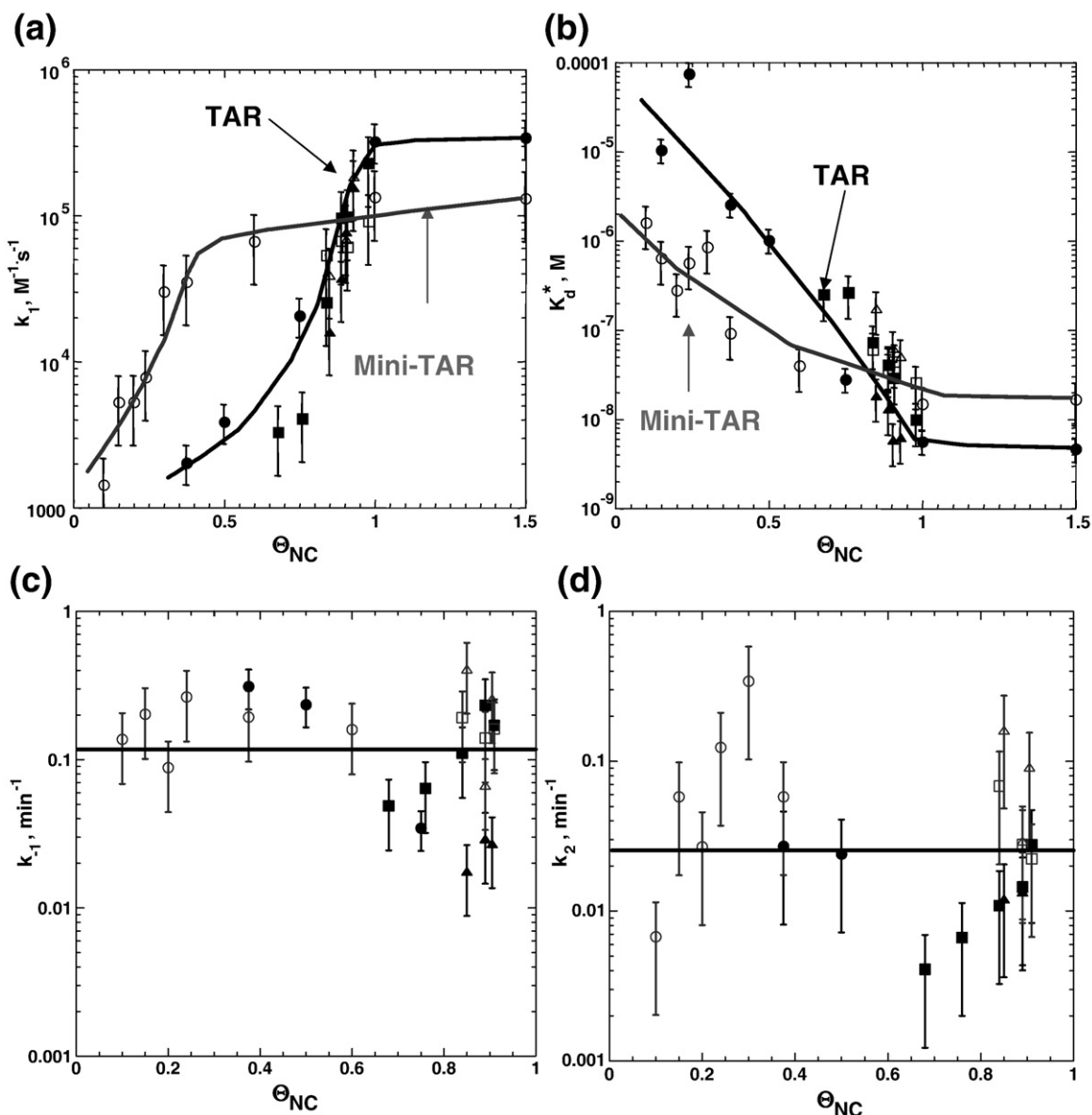


**Fig. 6.** Elementary rate analyses of mini-TAR (gray lines and symbols) and full-length TAR (black lines and symbols) RNA/DNA annealing as a function of fractional NC binding,  $\Theta_{NC}$ . The elementary reaction rates,  $k_1$  (a),  $K_d^*$  (b),  $k_{-1}$  (c), and  $k_2$  (d), were determined using Eqs. (3) and (4) based on three independent sets of experiments: titration of NC with no  $MgCl_2$  (Fig. 3), titration of NC with 1 mM  $MgCl_2$  (Fig. 4a and b), and titration of  $MgCl_2$  with 5  $\mu M$  NC (Fig. 4c and d).  $\Theta_{NC}$  was estimated using Eq. (2) for the assays with no  $MgCl_2$ . For the assays performed in the presence of  $Mg^{2+}$ ,  $\Theta_{NC}$  was estimated for each set of NC and  $MgCl_2$  concentrations assuming nonspecific electrostatic binding of NC and  $MgCl_2$  to NA using Eqs. (A1)–(A3) in the Supplementary Material. Symbols represent data obtained from titration of NC with no  $MgCl_2$  (circles) and with 1 mM  $MgCl_2$  (squares) and from titration of  $MgCl_2$  with 5  $\mu M$  NC (triangles). Open symbols represent mini-TAR and filled symbols represent full-length TAR annealing. Lines are guides for the eye.

result, these cations only facilitate  $k_1$  by a factor of  $\sim 10$  (Fig. 3a). In contrast, saturating NC induces  $\sim 10^2$ - and  $\sim 10^3$ -fold enhancement of  $k_1$  for mini-TAR and TAR, respectively (Fig. 6a). This effect is most likely the result of two NC properties. First, while  $Mg^{2+}$  and  $Na^+$  are only capable of screening NA–NA repulsion, NC additionally induces NA–NA attraction (i.e., aggregation), thereby efficiently facilitating the diffusional search for the complementary sequences. Second, while  $Mg^{2+}$  and  $Na^+$  stabilize NA duplexes, thereby slowing down melting of parts of hairpin structures that are in pre-

equilibrium to intermediate complex formation, NC destabilizes NA duplexes, thus facilitating intermediate formation.

An approximately 10-fold slower association rate of the longer TAR hairpins relative to the mini-TAR hairpins was observed at  $\Theta_{NC} \leq 0.5$ . This difference may be attributed to a larger entropy loss upon intermediate complex formation between longer hairpins under nonaggregating solution conditions. However, at  $\Theta_{NC} \sim 0.8$ ,  $k_1$  for TAR becomes larger and saturates at a value of  $\Theta_{NC} \sim 1$ , which is  $\sim 5$ -fold higher than that for mini-TAR (Fig. 6a). This

difference is most likely due to more facile premelting of the critical region involved in intermediate complex nucleation in TAR compared to mini-TAR hairpins and is consistent with the conclusion that mini-TAR and full-length TAR hairpins anneal via different pathways when saturated with NC.<sup>77</sup>

#### Effect of NC on the intermediate dissociation rate

Interestingly,  $k_{-1}$  is much less sensitive to variations in  $\Theta_{NC}$  than  $k_1$  (Fig. 6c). Moreover, the  $k_{-1}$  values for mini-TAR and full-length TAR are almost indistinguishable within the accuracy of the measurements. The average  $k_{-1}$  value over all measurements in the presence of NC ( $k_{-1}=0.12\pm 0.05\text{ min}^{-1}$ ) is 3-fold higher than the value determined in the absence of NC ( $k_{-1}=0.04\pm 0.01\text{ min}^{-1}$ ) (compare Figs. 3c and 6c). The  $k_{-1}$  values obtained from assays performed in the absence of  $Mg^{2+}$  (Fig. 6c, circles) are slightly higher than the values measured with  $Mg^{2+}$  (Fig. 6c, squares) but do not show significant variation with  $\Theta_{NC}$ . In contrast, the  $k_{-1}$  values obtained from assays performed with TAR in the presence of 1 mM  $Mg^{2+}$  (Fig. 6c, squares) increase by  $\sim 4$ -fold over the range of  $\Theta_{NC}$  values examined, while assays performed at 5  $\mu\text{M}$  NC and titrated with up to 100 mM  $Mg^{2+}$  (Fig. 6c, triangles) increase  $\sim 5$ -fold. This is consistent with the observation that higher  $Mg^{2+}$  results in slower duplex dissociation (see Fig. 3c). The facilitating effect of NC on  $k_{-1}$ , expected based on NC's duplex destabilizing ability,<sup>18,58</sup> may be obscured by a change in the annealing pathway from a kissing loop intermediate to a zipper intermediate at high NC.<sup>58,77</sup>

#### NC's effect on the intermediate dissociation constant

The  $\Theta_{NC}$  dependence on  $K_d^*$  (Fig. 6b) displays the opposite trend of  $k_1$  (Fig. 6a and b).  $K_d^*$  values vary between  $\sim 3\times 10^{-6}$  and  $2\times 10^{-8}$  M for the mini-TAR hairpins, while the variation for the full-length hairpin is much larger, that is, between  $\sim 10^{-4}$  and  $\sim 3\times 10^{-9}$  M. As observed in the absence of NC, at low  $\Theta_{NC}$ , the  $K_d^*$  values measured for TAR hairpins are  $\sim 10$ -fold higher than those for mini-TAR. However, at  $\Theta_{NC}\geq 0.8$ , the stability of the TAR intermediate equals that of the mini-TAR hairpins, and at saturating NC, the stability of the TAR intermediate exceeds that of the mini-TAR hairpins (see Fig. 6b). This likely reflects the fact that full-length TAR and mini-TAR hairpins anneal via different pathways at saturating NC.<sup>58,77</sup>

#### NC's effect on the strand-exchange rate

The  $k_2$  values display the largest scatter and show only a weak growth trend with increasing NC saturation,  $\Theta_{NC}$  (Fig. 6d). The  $k_2$  values at low NC saturation vary between the assays and decrease with  $Mg^{2+}$ , in accord with the data presented in Fig. 3d.

Importantly, the  $k_2$  values for mini-TAR and full-length TAR RNA/DNA annealing are similar, just as in the absence of NC. Also, the fact that the strand-exchange rate does not depend on the stem length suggests that the rate-limiting step of strand exchange involves a conformational change preceding base-pair zippering through the stem. On average, the measured  $k_2$  value is  $\sim 2$ - to 3-fold lower than  $k_{-1}$ . This result is in accord with the fact that formation of the reaction intermediate is in pre-equilibrium to strand exchange at all NC concentrations. The average  $k_2$  in the presence of NC ( $0.03\pm 0.01\text{ min}^{-1}$ ) is  $\sim 3$ -fold faster than in the absence of NC (compare Figs. 3d and 6d).

#### Mini-TAR and TAR aggregation by NC

NC induces NA aggregation, and NA saturation with NC is required for maximal aggregation activity.<sup>18,27,29,34,47–49,58</sup> The latter is a major component of the NA chaperone activity of NC<sup>58,77,95</sup> and facilitates efficient reverse transcription of long DNA products *in vitro*.<sup>96,97</sup>

To quantitatively test the hypothesis that NC-induced NA self-attraction is correlated with  $\Theta_{NC}$ , and to determine the strength of this attraction, we systematically studied the dependence of fractional NA aggregation,  $f_a$ , on  $\Theta_{NC}$  for mini-TAR and TAR. The conditions of the sedimentation assay were chosen to closely mimic our standard annealing assays. Presented in Fig. 7a are the results of an NC titration in the presence of 20 mM NaCl and no  $Mg^{2+}$ . The fraction of RNA aggregated,  $f_a$ , is plotted as a function of  $\Theta_{NC}$  determined according to Eq. (7). Interestingly, the aggregated fraction of NA approximately equals the fractional NC binding [compare the symbols (data points) and the line in Fig. 7a]; that is,  $f_a\approx\Theta_{NC}$ . These data are consistent with a 1:6 NC:nt binding at saturation, since aggregation is essentially complete, that is,  $f_a\approx 1$  at  $\Theta_{NC}\geq 1$  (Fig. 7a). It is important to note that the straight line is meant to be a guide to the eye, rather than a strict relationship. Although the sedimentation assay used here is not as accurate in quantifying the low fractional aggregation regime, the hint of the steeper dependence of  $f_a$  on  $\Theta_{NC}$  can be noticed around  $\Theta_{NC}\sim 0.6$ , in agreement with the notion that a critical amount of NC saturation is required for aggregation. Mini-TAR and TAR hairpins display similar aggregation behavior (Fig. 7a and b). However, a shorter 15-nt oligonucleotide under the same solution conditions remained unaggregated at all concentrations of NC tested (data not shown), in accord with the expectation that the specific level of NA saturation with NC leading to aggregation depends on the oligonucleotide length and concentration. The electrostatic mechanism of multivalent cation-induced NA aggregation leading to such behavior is discussed in the Supplementary Material. This aggregation mechanism also suggests different saturation requirements for aggregation with cationic proteins possessing different charge distributions.

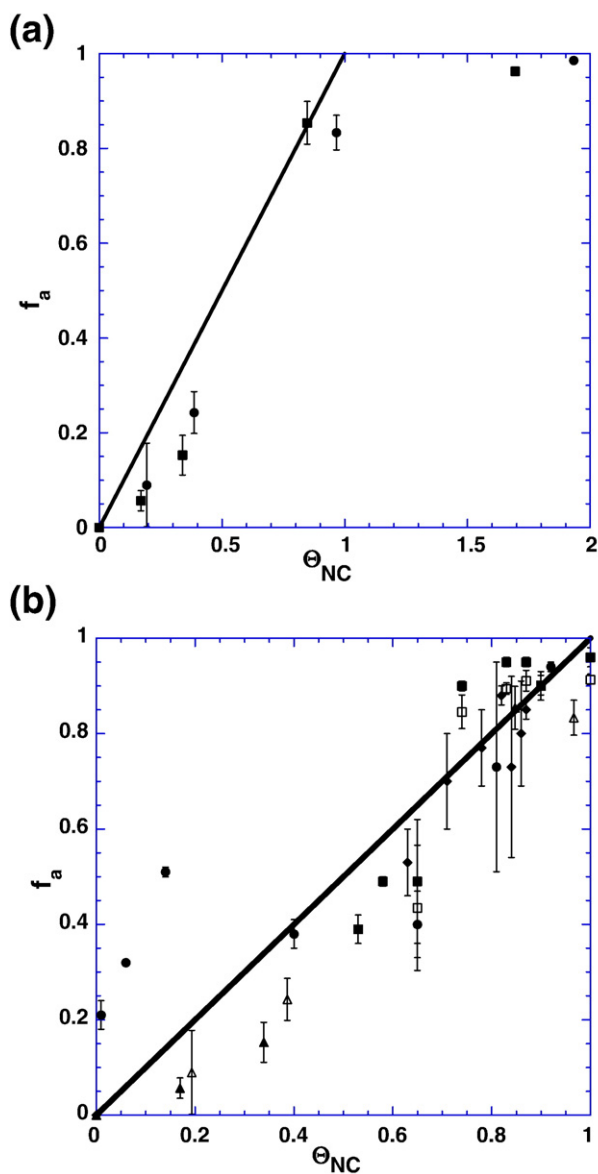


**Fig. 7.** Dependence of fraction of mini-TAR and full-length TAR RNA aggregated,  $f_a$ , on fractional NC binding,  $\Theta_{NC}$ . (a) Experimental  $f_a$  values obtained in sedimentation experiments performed in the absence of  $Mg^{2+}$ .  $\Theta_{NC}$  was calculated according to Eq. (7). RNA aggregation for either mini-TAR (circles) or full-length TAR (squares) saturates upon NA saturation with NC, that is, at  $\Theta_{NC} \geq 1$ . (b) Plot of the  $f_a$  versus  $\Theta_{NC}$  values from (a) (triangles), along with the results of additional sedimentation experiments: NC titration in the presence of 5 mM  $Mg^{2+}$  (circles), as well as  $Mg^{2+}$  (squares) or  $Na^+$  (diamonds) titration in the presence of 5  $\mu$ M NC. In (b), open symbols correspond to mini-TAR and filled symbols correspond to full-length TAR substrates. The straight line in both panels corresponds to  $f_a = \Theta_{NC}$ .

#### Mini-TAR and TAR aggregation in mixed NC/ $Mg^{2+}$ solutions

The fractional NA aggregation was also monitored as a function of  $\Theta_{NC}$  under conditions of mixed NC/ $Mg^{2+}$ / $Na^+$ . In one experiment,  $Mg^{2+}$

concentration was fixed at 5 mM and NC was titrated in the range of 1–30  $\mu$ M. In another set of experiments, NC was fixed at 5  $\mu$ M and either  $Mg^{2+}$  (in the range of 0.5–10 mM) or  $Na^+$  (in the range of 100–1000 mM) was varied. As discussed in more detail in the Supplementary Material, these data suggest that the nonelectrostatic component of binding free energy of NC to NA is  $\sim -5$  kcal/mol.

Mini-TAR and full-length TAR aggregation data are plotted as  $f_a$  versus  $\Theta_{NC}$  for all of the experiments performed either with or without  $Mg^{2+}$  or  $Na^+$  (Fig. 7b). All  $f_a$  ( $\Theta_{NC}$ ) dependencies follow approximately the relationship  $f_a \approx \Theta_{NC}$ . This result suggests that the fractional RNA aggregation in all of these assays is an approximate measure of the fractional NC binding. Also, these data support the conclusion that the electrostatic competition between NC and  $Mg^{2+}$  or  $Na^+$  cations according to Eqs. (A2) and (A3) indeed governs both NC binding and NC-induced NA aggregation.

## Conclusions

We previously showed that in the absence of NC, the mini-TAR<sup>58</sup> and full-length TAR<sup>77</sup> hairpins anneal via an extended kissing loop intermediate that involves 17 intermolecular base pairs (see Fig. 1, lower left). Here, we demonstrate that  $k_1$  is significantly facilitated by either  $Na^+$  or  $Mg^{2+}$  cations, although  $\sim 100$ -fold higher  $Na^+$  is required to produce the same effect. Saturated NC binding enhances  $k_1$  by 100-fold for mini-TAR and by  $10^4$ -fold for full-length TAR hairpins, far exceeding the maximal effect of  $Na^+$  and  $Mg^{2+}$  cations (Fig. 6a). We show that this NC effect on  $k_1$  is related to its ability to aggregate NAs (Fig. 7). In addition, in contrast to  $Na^+$  and  $Mg^{2+}$  cations, which reduce  $k_{-1}$  and  $k_2$  rates by a few fold (Fig. 3c and d), NC moderately facilitates these rates due to its ability to destabilize NA duplexes.<sup>32,37,38,40,41,44,46,53,55</sup> However, the full effect of NC on  $k_2$  in our study is partially masked by the fact that increasing NC also leads to a switch in the annealing pathway from kissing to zipper nucleation.<sup>77</sup>

We also show that the effect of  $Na^+$  and  $Mg^{2+}$  cations on the chaperone activity of NC is a result of nonspecific electrostatic competition for binding to NA. The kinetics is similar under solution conditions that lead to equivalent levels of NC binding to NA (Fig. 6). NC behaves effectively as a trivalent cation, with an additional nonelectrostatic binding free energy of  $\sim 5$  kcal/mol of protein, as discussed in the Supplementary Material.<sup>98–101</sup> This result provides additional support for the hypothesis that NC promotes NA aggregation via a similar electrostatic mechanism as other multivalent cations.<sup>102</sup>

Since NA aggregation<sup>47–49</sup> is a sequence-nonspecific property of NC, we expect these conclusions to hold for the majority of NA sequences. This is consistent with NC's role in facilitating multiple random strand transfer events during reverse transcription *in vivo*.<sup>26,60,62,103,104</sup> It is also in agreement

with the observation that formation of long reverse transcription products *in vitro* is facilitated under conditions of NC-induced RNA aggregation.<sup>96,97</sup> Based on the estimated NC concentration within the capsid core (~10 mM), NC and viral RNA are expected to be in an aggregated state and it is likely that at least the early stages of reverse transcription occur within this closely packed nucleoprotein complex. It remains an open question whether *in vivo* reverse transcription happens entirely within the RNA/NC aggregate. The traditional view is that the mature HIV-1 capsid disintegrates, that is, uncoats, prior to the beginning of reverse transcription.<sup>103</sup> However, uncoating is expected to dissolve the RNA/NC aggregate since the equilibrium solution conditions within the cytoplasm correspond to relatively high  $Mg^{2+}$  (i.e., low millimolar levels) compared to low NC concentration (i.e., below nanomolar levels). Under these conditions, strand transfer events would not be strongly promoted. On the other hand, if the capsid remains largely intact during reverse transcription and permeable to small ions and nucleotides, but not to the proteins (NC, RT, IN, etc.), then the millimolar concentration of NC present is expected to promote reverse transcription under aggregating conditions. The latter scenario is favored by a recent report showing that the decrease in capsid stability induced either by capsid protein mutations<sup>105,106</sup> or by the restriction factor Trim5 $\alpha$ <sup>107-109</sup> leads to a strong inhibition of reverse transcription. Therefore, the solution conditions that promote the formation of RNA/NC aggregates studied in this work may be relevant for *in vivo* reverse transcription.

## Materials and Methods

### Protein and NA preparation

The NC protein used in this work was prepared by solid-phase synthesis as previously described,<sup>110</sup> and its purity was estimated to be >95% by SDS-polyacrylamide gel electrophoresis. The concentration of NC was determined by measuring its absorbance at 280 nm and using  $\epsilon_{280} = 6050 \text{ mol}^{-1} \text{ cm}^{-1}$ .

All DNA oligonucleotides were purchased from Integrated DNA Technologies (Coralville, IA). Mini-TAR RNA (27 nt) was obtained from Dharmacon RNA Technologies (Lafayette, CO). Full-length TAR RNA (59 nt) was generated by *in vitro* transcription.

The concentrations of the RNA and DNA oligonucleotides were determined by measuring their absorbances at 260 nm. The following extinction coefficients were used: mini-TAR RNA (27-mer),  $2.82 \times 10^5 \text{ M}^{-1} \text{ cm}^{-1}$ ; mini-TAR DNA (32-mer),  $3.06 \times 10^5 \text{ M}^{-1} \text{ cm}^{-1}$ ; TAR RNA (59-mer),  $5.34 \times 10^5 \text{ M}^{-1} \text{ cm}^{-1}$ ; TAR DNA (59-mer),  $5.65 \times 10^5 \text{ M}^{-1} \text{ cm}^{-1}$ .

Prior to use, all oligonucleotides were refolded in 25 mM Hepes, pH7.5, and 100 mM NaCl at a concentration 100 $\times$  that used in the annealing reactions. This was accomplished by incubation at 80 °C for 2 min and cooling to 60 °C for 2 min followed by addition of  $MgCl_2$  to a final concentration of 10 mM and placement on ice.

### Annealing assays

For annealing assays, refolded <sup>32</sup>P-labeled RNA (mini-TAR RNA or full-length TAR RNA) was combined with unlabeled complementary DNA in a solution containing 20 mM Hepes (pH7.5), 20 mM NaCl, and 0.2 mM  $MgCl_2$ , at 37 °C, except when otherwise indicated.

In the absence of NC, studies of the  $Na^+$  and  $Mg^{2+}$  dependence of annealing were performed with 15 nM RNA and 500 nM complementary DNA in the presence of various concentrations of NaCl or  $MgCl_2$ , as indicated in the figure legends. Reactions were initiated by adding DNA to RNA, followed by incubation in the reaction buffer for the indicated time. Reactions were quenched by placing solutions on ice followed by addition of glycerol to 5% final volume. Samples were analyzed on 15% or 12% SDS-polyacrylamide gels for mini-TAR and full-length TAR annealing, respectively.

Studies of the NC concentration dependence of annealing were performed by mixing 15 nM RNA and 150 nM complementary DNA. Reactions were initiated by adding NC to final concentrations indicated in the figure legends, followed by incubation in the reaction buffer for the indicated time. In these experiments, the only  $Mg^{2+}$  in the final reaction buffer was the amount present due to the RNA and DNA refolding procedure described above (~0.2 mM final). Studies of the  $Mg^{2+}$  dependence of annealing in the presence of NC were performed by incubating 15 nM RNA with 90 nM DNA in the presence of various  $[Mg^{2+}]$ , as indicated in the figure legends, prior to the addition of 5  $\mu$ M NC. Annealing reactions were quenched at the indicated times by incubation with 1% (w/v) SDS on ice for 5 min. Samples were subjected to phenol/chloroform extraction (2 $\times$ ), followed by addition of glycerol to 5% final volume and analysis on SDS-polyacrylamide gels as described above. All gels were visualized using a Bio-Rad Molecular Imager FX and quantified with Bio-Rad Quantity One Software.

The NC concentration dependence of annealing in the presence of 1 mM  $Mg^{2+}$  was carried out with 15 nM RNA and 90 nM DNA in the presence of four different concentrations of NC (2, 5, 10, and 20  $\mu$ M). All of these NC concentrations correspond to an nt:NC ratio < 1, that is, to the large excess of NC, required for NC/NA binding due to high  $[Mg^{2+}]$ . The annealing reactions were performed and analyzed as described above.

### Sedimentation/aggregation assays

Refolded <sup>32</sup>P-labeled mini-TAR or full-length TAR RNA (15 nM) was combined with complementary DNA oligonucleotides (100 nM mini-TAR DNA or 45 nM full-length TAR DNA) in a solution containing 20 mM Hepes (pH7.5), 20 mM NaCl, and 0.2 mM  $MgCl_2$ . NC was added to final concentrations of 0.1, 0.2, 0.5, 1.0, or 2.0  $\mu$ M, and reactions (40  $\mu$ L) were incubated at 37 °C for 30 min. For NC/ $Mg^{2+}$  or NC/ $Na^+$  competition assays, 0–20 mM  $Mg^{2+}$  or 0–1000 mM  $Na^+$  was titrated in the presence of 5.0  $\mu$ M NC. Assays were also performed in the presence of a fixed concentration of 5 mM  $Mg^{2+}$  and varying concentrations of NC (0 to 30  $\mu$ M). At the end of the incubation period, solutions were centrifuged at 12,000 rpm in a microcentrifuge for 20 min. Supernatant (5  $\mu$ L) was collected and analyzed by scintillation counting. The fraction of radioactivity remaining in the supernatant relative to the RNA-only sample (set to 1) was plotted as a function of fractional NC binding,  $\Theta_{NC}$ .

## Acknowledgements

We would like to thank Drs. Daniel G. Mullen and Brandie Kovaleski (University of Minnesota) for chemical synthesis of NC. This research was supported by National Institutes of Health grant GM065056 (K.M.-F.) and by National Institutes of Health predoctoral training grant T32 GM008700 awarded to M.-N.V.

## Supplementary Data

Supplementary data associated with this article can be found, in the online version, at [doi:10.1016/j.jmb.2008.12.073](https://doi.org/10.1016/j.jmb.2008.12.073)

## References

- Henderson, L. E., Bowers, M. A., Sowder, R. C., II, Serabyn, S. A., Johnson, D. G., Bess, J. W., Jr. *et al.* (1992). Gag proteins of the highly replicative MN strain of human immunodeficiency virus type 1: posttranslational modifications, proteolytic processings, and complete amino acid sequences. *J. Virol.* **66**, 1856–1865.
- Tritch, R. J., Cheng, Y. E., Yin, F. H. & Erickson-Viitanen, S. (1991). Mutagenesis of protease cleavage sites in the human immunodeficiency virus type 1 gag polyprotein. *J. Virol.* **65**, 922–930.
- Veronese, F. D., Rahman, R., Copeland, T. D., Oroszlan, S., Gallo, R. C. & Sarngadharan, M. G. (1987). Immunological and chemical analysis of P6, the carboxyl-terminal fragment of HIV P15. *AIDS Res. Hum. Retroviruses*, **3**, 253–264.
- Dupraz, P., Oertle, S., Meric, C., Damay, P. & Spahr, P. F. (1990). Point mutations in the proximal Cys-His box of Rous sarcoma virus nucleocapsid protein. *J. Virol.* **64**, 4978–4987.
- Rein, A. (1994). Retroviral RNA packaging: a review. *Arch. Virol., Suppl.* **9**, 513–522.
- Hibbert, C. S., Mirro, J. & Rein, A. (2004). mRNA molecules containing murine leukemia virus packaging signals are encapsidated as dimers. *J. Virol.* **78**, 10927–10938.
- Muriaux, D., Mirro, J., Nagashima, K., Harvin, D. & Rein, A. (2002). Murine leukemia virus nucleocapsid mutant particles lacking viral RNA encapsidate ribosomes. *J. Virol.* **76**, 11405–11413.
- Rulli, S. J., Jr., Hibbert, C. S., Mirro, J., Pederson, T., Biswal, S. & Rein, A. (2007). Selective and non-selective packaging of cellular RNAs in retrovirus particles. *J. Virol.* **81**, 6623–6631.
- Ako-Adjei, D., Johnson, M. C. & Vogt, V. M. (2005). The retroviral capsid domain dictates virion size, morphology, and coassembly of gag into virus-like particles. *J. Virol.* **79**, 13463–13472.
- Briggs, J. A., Johnson, M. C., Simon, M. N., Fuller, S. D. & Vogt, V. M. (2006). Cryo-electron microscopy reveals conserved and divergent features of gag packing in immature particles of Rous sarcoma virus and human immunodeficiency virus. *J. Mol. Biol.* **355**, 157–168.
- Briggs, J. A., Simon, M. N., Gross, I., Krausslich, H. G., Fuller, S. D., Vogt, V. M. & Johnson, M. C. (2004). The stoichiometry of Gag protein in HIV-1. *Nat. Struct. Mol. Biol.* **11**, 672–675.
- Muriaux, D., Mirro, J., Harvin, D. & Rein, A. (2001). RNA is a structural element in retrovirus particles. *Proc. Natl Acad. Sci. USA*, **98**, 5246–5251.
- Prats, A. C., Housset, V., de Billy, G., Cornille, F., Prats, H., Roques, B. & Darlix, J. L. (1991). Viral RNA annealing activities of the nucleocapsid protein of Moloney murine leukemia virus are zinc independent. *Nucleic Acids Res.* **19**, 3533–3541.
- Weiss, S., Konig, B., Morikawa, Y. & Jones, I. (1992). Recombinant HIV-1 nucleocapsid protein p15 produced as a fusion protein with glutathione S-transferase in *Escherichia coli* mediates dimerization and enhances reverse transcription of retroviral RNA. *Gene*, **121**, 203–212.
- Baba, S., Takahashi, K., Koyanagi, Y., Yamamoto, N., Takaku, H., Gorelick, R. J. & Kawai, G. (2003). Role of the zinc fingers of HIV-1 nucleocapsid protein in maturation of genomic RNA. *J. Biochem. (Tokyo)*, **134**, 637–639.
- Feng, Y. X., Copeland, T. D., Henderson, L. E., Gorelick, R. J., Bosche, W. J., Levin, J. G. & Rein, A. (1996). HIV-1 nucleocapsid protein induces “maturation” of dimeric retroviral RNA in vitro. *Proc. Natl Acad. Sci. USA*, **93**, 7577–7581.
- Barat, C., Lullien, V., Schatz, O., Keith, G., Nugeyre, M. T., Gruninger-Leitch, F. *et al.* (1989). HIV-1 reverse transcriptase specifically interacts with the anticodon domain of its cognate primer tRNA. *EMBO J.* **8**, 3279–3285.
- Hargittai, M. R., Gorelick, R. J., Rouzina, I. & Musier-Forsyth, K. (2004). Mechanistic insights into the kinetics of HIV-1 nucleocapsid protein-facilitated tRNA annealing to the primer binding site. *J. Mol. Biol.* **337**, 951–968.
- Khan, R. & Giedroc, D. P. (1992). Recombinant human immunodeficiency virus type 1 nucleocapsid (NCp7) protein unwinds tRNA. *J. Biol. Chem.* **267**, 6689–6695.
- Tisne, C., Roques, B. P. & Dardel, F. (2004). The annealing mechanism of HIV-1 reverse transcription primer onto the viral genome. *J. Biol. Chem.* **279**, 3588–3595.
- Levin, J. G., Guo, J., Rouzina, I. & Musier-Forsyth, K. (2005). Nucleic acid chaperone activity of HIV-1 nucleocapsid protein: critical role in reverse transcription and molecular mechanism. *Prog. Nucleic Acid Res. Mol. Biol.* **80**, 217–286.
- Thomas, J. A., Gagliardi, T. D., Alvord, W. G., Lubomirski, M., Bosche, W. J. & Gorelick, R. J. (2006). Human immunodeficiency virus type 1 nucleocapsid zinc-finger mutations cause defects in reverse transcription and integration. *Virology*, **353**, 41–51.
- Thomas, J. A. & Gorelick, R. J. (2008). Nucleocapsid protein function in early infection processes. *Virus Res.* **134**, 39–63.
- Thomas, J. A., Shulenin, S., Coren, L. V., Bosche, W. J., Gagliardi, T. D., Gorelick, R. J. & Oroszlan, S. (2006). Characterization of human immunodeficiency virus type 1 (HIV-1) containing mutations in the nucleocapsid protein at a putative HIV-1 protease cleavage site. *Virology*, **354**, 261–270.
- Darlix, J. L., Lapadat-Tapolsky, M., de Rocquigny, H. & Roques, B. P. (1995). First glimpses at structure-function relationships of the nucleocapsid protein of retroviruses. *J. Mol. Biol.* **254**, 523–537.
- Rein, A., Henderson, L. E. & Levin, J. G. (1998). Nucleic-acid-chaperone activity of retroviral nucleocapsid proteins: significance for viral replication. *Trends Biochem. Sci.* **23**, 297–301.

27. Tsuchihashi, Z. & Brown, P. O. (1994). DNA strand exchange and selective DNA annealing promoted by the human immunodeficiency virus type 1 nucleocapsid protein. *J. Virol.* **68**, 5863–5870.
28. Dey, A., York, D., Smalls-Mantey, A. & Summers, M. F. (2005). Composition and sequence-dependent binding of RNA to the nucleocapsid protein of Moloney murine leukemia virus. *Biochemistry*, **44**, 3735–3744.
29. Dib-Hajj, F., Khan, R. & Giedroc, D. P. (1993). Retroviral nucleocapsid proteins possess potent nucleic acid strand renaturation activity. *Protein Sci.* **2**, 231–243.
30. Fisher, R. J., Rein, A., Fivash, M., Urbaneja, M. A., Casas-Finet, J. R., Medaglia, M. & Henderson, L. E. (1998). Sequence-specific binding of human immunodeficiency virus type 1 nucleocapsid protein to short oligonucleotides. *J. Virol.* **72**, 1902–1909.
31. Mély, Y., de Rocquigny, H., Sorinas-Jimeno, M., Keith, G., Roques, B. P., Marquet, R. & Gerard, D. (1995). Binding of the HIV-1 nucleocapsid protein to the primer tRNA(3Lys), in vitro, is essentially not specific. *J. Biol. Chem.* **270**, 1650–1656.
32. Urbaneja, M. A., Wu, M., Casas-Finet, J. R. & Karpel, R. L. (2002). HIV-1 nucleocapsid protein as a nucleic acid chaperone: spectroscopic study of its helix-destabilizing properties, structural binding specificity, and annealing activity. *J. Mol. Biol.* **318**, 749–764.
33. Vuilleumier, C., Bombarda, E., Morellet, N., Gerard, D., Roques, B. P. & Mély, Y. (1999). Nucleic acid sequence discrimination by the HIV-1 nucleocapsid protein NCp7: a fluorescence study. *Biochemistry*, **38**, 16816–16825.
34. Khan, R. & Giedroc, D. P. (1994). Nucleic acid binding properties of recombinant Zn2 HIV-1 nucleocapsid protein are modulated by COOH-terminal processing. *J. Biol. Chem.* **269**, 22538–22546.
35. You, J. C. & McHenry, C. S. (1993). HIV nucleocapsid protein. Expression in *Escherichia coli*, purification, and characterization. *J. Biol. Chem.* **268**, 16519–16527.
36. You, J. C. & McHenry, C. S. (1994). Human immunodeficiency virus nucleocapsid protein accelerates strand transfer of the terminally redundant sequences involved in reverse transcription. *J. Biol. Chem.* **269**, 31491–31495.
37. Azoulay, J., Clamme, J. P., Darlix, J. L., Roques, B. P. & Mély, Y. (2003). Destabilization of the HIV-1 complementary sequence of TAR by the nucleocapsid protein through activation of conformational fluctuations. *J. Mol. Biol.* **326**, 691–700.
38. Beltz, H., Azoulay, J., Bernacchi, S., Clamme, J. P., Ficheux, D., Roques, B. *et al.* (2003). Impact of the terminal bulges of HIV-1 cTAR DNA on its stability and the destabilizing activity of the nucleocapsid protein NCp7. *J. Mol. Biol.* **328**, 95–108.
39. Beltz, H., Clauss, C., Piemont, E., Ficheux, D., Gorelick, R. J., Roques, B. *et al.* (2005). Structural determinants of HIV-1 nucleocapsid protein for cTAR DNA binding and destabilization, and correlation with inhibition of self-primed DNA synthesis. *J. Mol. Biol.* **348**, 1113–1126.
40. Beltz, H., Piemont, E., Schaub, E., Ficheux, D., Roques, B., Darlix, J. L. & Mély, Y. (2004). Role of the structure of the top half of HIV-1 cTAR DNA on the nucleic acid destabilizing activity of the nucleocapsid protein NCp7. *J. Mol. Biol.* **338**, 711–723.
41. Bernacchi, S., Stoylov, S., Piemont, E., Ficheux, D., Roques, B. P., Darlix, J. L. & Mély, Y. (2002). HIV-1 nucleocapsid protein activates transient melting of least stable parts of the secondary structure of TAR and its complementary sequence. *J. Mol. Biol.* **317**, 385–399.
42. Egele, C., Schaub, E., Ramalanjaona, N., Piemont, E., Ficheux, D., Roques, B. *et al.* (2004). HIV-1 nucleocapsid protein binds to the viral DNA initiation sequences and chaperones their kissing interactions. *J. Mol. Biol.* **342**, 453–466.
43. Hong, M. K., Harbron, E. J., O'Connor, D. B., Guo, J., Barbara, P. F., Levin, J. G. & Musier-Forsyth, K. (2003). Nucleic acid conformational changes essential for HIV-1 nucleocapsid protein-mediated inhibition of self-priming in minus-strand transfer. *J. Mol. Biol.* **325**, 1–10.
44. Kankia, B. I., Barany, G. & Musier-Forsyth, K. (2005). Unfolding of DNA quadruplexes induced by HIV-1 nucleocapsid protein. *Nucleic Acids Res.* **33**, 4395–4403.
45. Liu, H. W., Zeng, Y., Landes, C. F., Kim, Y. J., Zhu, Y., Ma, X. *et al.* (2007). Inaugural article: insights on the role of nucleic acid/protein interactions in chaperoned nucleic acid rearrangements of HIV-1 reverse transcription. *Proc. Natl Acad. Sci. USA*, **104**, 5261–5267.
46. Williams, M. C., Rouzina, I., Wenner, J. R., Gorelick, R. J., Musier-Forsyth, K. & Bloomfield, V. A. (2001). Mechanism for nucleic acid chaperone activity of HIV-1 nucleocapsid protein revealed by single molecule stretching. *Proc. Natl Acad. Sci. USA*, **98**, 6121–6126.
47. Krishnamoorthy, G., Roques, B., Darlix, J. L. & Mély, Y. (2003). DNA condensation by the nucleocapsid protein of HIV-1: a mechanism ensuring DNA protection. *Nucleic Acids Res.* **31**, 5425–5432.
48. Le Cam, E., Coulaud, D., Delain, E., Petitjean, P., Roques, B. P., Gerard, D. *et al.* (1998). Properties and growth mechanism of the ordered aggregation of a model RNA by the HIV-1 nucleocapsid protein: an electron microscopy investigation. *Biopolymers*, **45**, 217–229.
49. Stoylov, S. P., Vuilleumier, C., Stoylova, E., De Rocquigny, H., Roques, B. P., Gerard, D. & Mély, Y. (1997). Ordered aggregation of ribonucleic acids by the human immunodeficiency virus type 1 nucleocapsid protein. *Biopolymers*, **41**, 301–312.
50. Guo, J., Wu, T., Anderson, J., Kane, B. F., Johnson, D. G., Gorelick, R. J. *et al.* (2000). Zinc finger structures in the human immunodeficiency virus type 1 nucleocapsid protein facilitate efficient minus- and plus-strand transfer. *J. Virol.* **74**, 8980–8988.
51. Heath, M. J., Derebail, S. S., Gorelick, R. J. & DeStefano, J. J. (2003). Differing roles of the N- and C-terminal zinc fingers in human immunodeficiency virus nucleocapsid protein-enhanced nucleic acid annealing. *J. Biol. Chem.* **278**, 30755–30763.
52. Narayanan, N., Gorelick, R. J. & DeStefano, J. J. (2006). Structure/function mapping of amino acids in the N-terminal zinc finger of the human immunodeficiency virus type 1 nucleocapsid protein: residues responsible for nucleic acid helix destabilizing activity. *Biochemistry*, **45**, 12617–12628.
53. Williams, M. C., Gorelick, R. J. & Musier-Forsyth, K. (2002). Specific zinc-finger architecture required for HIV-1 nucleocapsid protein's nucleic acid chaperone function. *Proc. Natl Acad. Sci. USA*, **99**, 8614–8619.
54. Cruceanu, M., Gorelick, R. J., Musier-Forsyth, K., Rouzina, I. & Williams, M. C. (2006). Rapid kinetics of protein–nucleic acid interaction is a major component of HIV-1 nucleocapsid protein's nucleic acid chaperone function. *J. Mol. Biol.* **363**, 867–877.

55. Cruceanu, M., Urbaneja, M. A., Hixson, C. V., Johnson, D. G., Datta, S. A., Fivash, M. J. *et al.* (2006). Nucleic acid binding and chaperone properties of HIV-1 Gag and nucleocapsid proteins. *Nucleic Acids Res.* **34**, 593–605.
56. DeStefano, J. J. (1995). Human immunodeficiency virus nucleocapsid protein stimulates strand transfer from internal regions of heteropolymeric RNA templates. *Arch. Virol.* **140**, 1775–1789.
57. Heath, M. J. & Destefano, J. J. (2005). A complementary single-stranded docking site is required for enhancement of strand exchange by human immunodeficiency virus nucleocapsid protein on substrates that model viral recombination. *Biochemistry*, **44**, 3915–3925.
58. Vo, M. N., Barany, G., Rouzina, I. & Musier-Forsyth, K. (2006). Mechanistic studies of mini-TAR RNA/DNA annealing in the absence and presence of HIV-1 nucleocapsid protein. *J. Mol. Biol.* **363**, 244–261.
59. Baird, H. A., Galetto, R., Gao, Y., Simon-Loriere, E., Abreha, M., Archer, J. *et al.* (2006). Sequence determinants of breakpoint location during HIV-1 intersubtype recombination. *Nucleic Acids Res.* **34**, 5203–5216.
60. Galetto, R. & Negroni, M. (2005). Mechanistic features of recombination in HIV. *AIDS Rev.* **7**, 92–102.
61. Johnson, P. E., Turner, R. B., Wu, Z. R., Hairston, L., Guo, J., Levin, J. G. & Summers, M. F. (2000). A mechanism for plus-strand transfer enhancement by the HIV-1 nucleocapsid protein during reverse transcription. *Biochemistry*, **39**, 9084–9091.
62. Negroni, M. & Buc, H. (1999). Recombination during reverse transcription: an evaluation of the role of the nucleocapsid protein. *J. Mol. Biol.* **286**, 15–31.
63. Roda, R. H., Balakrishnan, M., Hanson, M. N., Wohrl, B. M., Le Grice, S. F., Roques, B. P. *et al.* (2003). Role of the reverse transcriptase, nucleocapsid protein, and template structure in the two-step transfer mechanism in retroviral recombination. *J. Biol. Chem.* **278**, 31536–31546.
64. Rodriguez-Rodriguez, L., Tsuchihashi, Z., Fuentes, G. M., Bambara, R. A. & Fay, P. J. (1995). Influence of human immunodeficiency virus nucleocapsid protein on synthesis and strand transfer by the reverse transcriptase in vitro. *J. Biol. Chem.* **270**, 15005–15011.
65. Derebail, S. S., Heath, M. J. & DeStefano, J. J. (2003). Evidence for the differential effects of nucleocapsid protein on strand transfer in various regions of the HIV genome. *J. Biol. Chem.* **278**, 15702–15712.
66. Cosa, G., Harbron, E. J., Zeng, Y., Liu, H. W., O'Connor, D. B., Eta-Hosokawa, C. *et al.* (2004). Secondary structure and secondary structure dynamics of DNA hairpins complexed with HIV-1 NC protein. *Biophys. J.* **87**, 2759–2767.
67. Godet, J., de Rocquigny, H., Raja, C., Glasser, N., Ficheux, D., Darlix, J. L. & Mély, Y. (2006). During the early phase of HIV-1 DNA synthesis, nucleocapsid protein directs hybridization of the TAR complementary sequences via the ends of their double-stranded stem. *J. Mol. Biol.* **356**, 1180–1192.
68. Guo, J., Wu, T., Kane, B. F., Johnson, D. G., Henderson, L. E., Gorelick, R. J. & Levin, J. G. (2002). Subtle alterations of the native zinc finger structures have dramatic effects on the nucleic acid chaperone activity of human immunodeficiency virus type 1 nucleocapsid protein. *J. Virol.* **76**, 4370–4378.
69. Heilman-Miller, S. L., Wu, T. & Levin, J. G. (2004). Alteration of nucleic acid structure and stability modulates the efficiency of minus-strand transfer mediated by the HIV-1 nucleocapsid protein. *J. Biol. Chem.* **279**, 44154–44165.
70. Wu, T., Heilman-Miller, S. L. & Levin, J. G. (2007). Effects of nucleic acid local structure and magnesium ions on minus-strand transfer mediated by the nucleic acid chaperone activity of HIV-1 nucleocapsid protein. *Nucleic Acids Res.* **35**, 3974–3987.
71. Goldschmidt, V., Didierjean, J., Ehresmann, B., Ehresmann, C., Isel, C. & Marquet, R. (2006). Mg<sup>2+</sup> dependency of HIV-1 reverse transcription, inhibition by nucleoside analogues and resistance. *Nucleic Acids Res.* **34**, 42–52.
72. Cantor, C. R. & Schimmel, P. R. (1980). *Biophysical Chemistry. Part III. The Behavior of Biological Macromolecules*. W. H. Freeman & Co., San Francisco, CA.
73. Shubsda, M. F., McPike, M. P., Goodisman, J. & Dabrowiak, J. C. (1999). Monomer–dimer equilibrium constants of RNA in the dimer initiation site of human immunodeficiency virus type 1. *Biochemistry*, **38**, 10147–10157.
74. Bloomfield, V. A., Crothers, D. M. & Tinoco, I. (2000). *Nucleic Acids Structure, Properties, and Function*. University Science Books, Sausalito, CA.
75. Porschke, D. (1973). The dynamics of nucleic-acid single-strand conformation changes. Oligo- and polyriboadenylic acids. *Eur. J. Biochem.* **39**, 117–126.
76. Wetmur, J. G. & Davidson, N. (1968). Kinetics of renaturation of DNA. *J. Mol. Biol.* **31**, 349–370.
77. Vo, M. N., Barany, G., Rouzina, I. & Musier-Forsyth, K. (2009). HIV-1 nucleocapsid protein switches the pathway of Transactivation Response Element RNA/DNA annealing from loop–loop “kissing” to “zipper”. *J. Mol. Biol.* **386**, 789–801.
78. Lohman, T. M., DeHaseth, P. L. & Record, M. T., Jr. (1978). Analysis of ion concentration effects of the kinetics of protein–nucleic acid interactions. Application to lac repressor–operator interactions. *Biophys. Chem.* **8**, 281–294.
79. Bokinsky, G., Rueda, D., Misra, V. K., Rhodes, M. M., Gordus, A., Babcock, H. P. *et al.* (2003). Single-molecule transition-state analysis of RNA folding. *Proc. Natl Acad. Sci. USA*, **100**, 9302–9307.
80. Manning, G. S. (1976). On the application of polyelectrolyte limiting laws to the helix-coil transition of DNA. V. Ionic effects on renaturation kinetics. *Biopolymers*, **15**, 1333–1343.
81. Williams, A. P., Longfellow, C. E., Freier, S. M., Kierzek, R. & Turner, D. H. (1989). Laser temperature-jump, spectroscopic, and thermodynamic study of salt effects on duplex formation by dGCATGC. *Biochemistry*, **28**, 4283–4291.
82. Jossinet, F., Paillart, J. C., Westhof, E., Hermann, T., Skripkin, E., Lodmell, J. S. *et al.* (1999). Dimerization of HIV-1 genomic RNA of subtypes A and B: RNA loop structure and magnesium binding. *RNA*, **5**, 1222–1234.
83. Gregorian, R. S., Jr. & Crothers, D. M. (1995). Determinants of RNA hairpin loop–loop complex stability. *J. Mol. Biol.* **248**, 968–984.
84. Marino, J. P., Gregorian, R. S., Jr., Csankovszki, G. & Crothers, D. M. (1995). Bent helix formation between RNA hairpins with complementary loops. *Science*, **268**, 1448–1454.
85. Blagoi, Y. P., Sorokin, V. A., Valeyev, V. A., Khomenko, S. A. & Gladchenko, G. O. (1978). Magnesium ion effect on the helix-coil transition of DNA. *Biopolymers*, **17**, 1103–1118.
86. Krakauer, H. (1974). A thermodynamic analysis of the influence of simple mono- and divalent cations

- on the conformational transitions of polynucleotide complexes. *Biochemistry*, **13**, 2579–2589.
87. Weixlbaumer, A., Werner, A., Flamm, C., Westhof, E. & Schroeder, R. (2004). Determination of thermodynamic parameters for HIV DIS type loop–loop kissing complexes. *Nucleic Acids Res.* **32**, 5126–5133.
  88. Frank-Kamenetskii, F. (1971). Simplification of the empirical relationship between melting temperature of DNA, its GC content and concentration of sodium ions in solution. *Biopolymers*, **10**, 2623–2624.
  89. Shubsda, M., Goodisman, J. & Dabrowiak, J. C. (1999). Characterization of hairpin-duplex interconversion of DNA using polyacrylamide gel electrophoresis. *Biophys. Chem.* **76**, 95–115.
  90. Hohng, S., Wilson, T. J., Tan, E., Clegg, R. M., Lilley, D. M. & Ha, T. (2004). Conformational flexibility of four-way junctions in RNA. *J. Mol. Biol.* **336**, 69–79.
  91. Joo, C., McKinney, S. A., Lilley, D. M. & Ha, T. (2004). Exploring rare conformational species and ionic effects in DNA Holliday junctions using single-molecule spectroscopy. *J. Mol. Biol.* **341**, 739–751.
  92. Karymov, M., Daniel, D., Sankey, O. F. & Lyubchenko, Y. L. (2005). Holliday junction dynamics and branch migration: single-molecule analysis. *Proc. Natl Acad. Sci. USA*, **102**, 8186–8191.
  93. McKinney, S. A., Tan, E., Wilson, T. J., Nahas, M. K., Declais, A. C., Clegg, R. M. *et al.* (2004). Single-molecule studies of DNA and RNA four-way junctions. *Biochem. Soc. Trans.* **32**, 41–45.
  94. Paoletti, A. C., Shubsda, M. F., Hudson, B. S. & Borer, P. N. (2002). Affinities of the nucleocapsid protein for variants of SL3 RNA in HIV-1. *Biochemistry*, **41**, 15423–15428.
  95. Stewart-Maynard, K. M., Cruceanu, M., Wang, F., Vo, M.-N., Gorelick, R. J., Williams, M. C. *et al.* (2008). Retroviral nucleocapsid proteins display non-equivalent levels of nucleic acid chaperone activity. *J. Virol.* **82**, 10129–10142.
  96. Anthony, R. M. & Destefano, J. J. (2007). In vitro synthesis of long DNA products in reactions with HIV-RT and nucleocapsid protein. *J. Mol. Biol.* **365**, 310–324.
  97. Mirambeau, G., Lyonnais, S., Coulaud, D., Hameau, L., Lafosse, S., Jeusset, J. *et al.* (2007). HIV-1 protease and reverse transcriptase control the architecture of their nucleocapsid partner. *PLoS ONE*, **2**, e669.
  98. Yuan, Y., Kerwood, D. J., Paoletti, A. C., Shubsda, M. F. & Borer, P. N. (2003). Stem of SL1 RNA in HIV-1: structure and nucleocapsid protein binding for a  $1 \times 3$  internal loop. *Biochemistry*, **42**, 5259–5269.
  99. Nguyen, T. T., Rouzina, I. & Shklovskii, B. I. (2000). Reentrant condensation of DNA induced by multivalent counterions. *J. Chem. Phys.* **112**, 2562–2568.
  100. Rouzina, I. & Bloomfield, V. A. (1996). Macroion attraction due to electrostatic correlation between screening counterions. 1. Mobile surface-adsorbed ions and diffuse ion cloud. *J. Phys. Chem.* **100**, 9977–9989.
  101. Zhang, R. & Shklovskii, B. I. (2004). Phase diagram of aggregation of oppositely charged colloids in salty water. *Phys. Rev., E Stat. Nonlinear Soft Matter Phys.* **69**, 021909.
  102. Bloomfield, V. A. (1997). DNA condensation by multivalent cations. *Biopolymers*, **44**, 269–282.
  103. Coffin, J. M., Hughes, S. H. & Varmus, H. E. (1997). Retroviruses. Cold Spring Harbor Laboratory Press, Cold Spring Harbor, NY.
  104. Hu, W. S., Rhodes, T., Dang, Q. & Pathak, V. (2003). Retroviral recombination: review of genetic analyses. *Front. Biosci.* **8**, d143–d155.
  105. Forshey, B. M., von Schwedler, U., Sundquist, W. I. & Aiken, C. (2002). Formation of a human immunodeficiency virus type 1 core of optimal stability is crucial for viral replication. *J. Virol.* **76**, 5667–5677.
  106. Ganser-Pornillos, B. K., Yeager, M. & Sundquist, W. I. (2008). The structural biology of HIV assembly. *Curr. Opin. Struct. Biol.* **18**, 203–217.
  107. Diaz-Griffero, F., Perron, M., McGee-Estrada, K., Hanna, R., Maillard, P. V., Trono, D. & Sodroski, J. (2008). A human TRIM5alpha B30.2/SPRY domain mutant gains the ability to restrict and prematurely uncoat B-tropic murine leukemia virus. *Virology*, **378**, 233–242.
  108. Perron, M. J., Stremlau, M., Lee, M., Javanbakht, H., Song, B. & Sodroski, J. (2007). The human TRIM5alpha restriction factor mediates accelerated uncoating of the N-tropic murine leukemia virus capsid. *J. Virol.* **81**, 2138–2148.
  109. Stremlau, M., Perron, M., Welikala, S. & Sodroski, J. (2005). Species-specific variation in the B30.2(SPRY) domain of TRIM5alpha determines the potency of human immunodeficiency virus restriction. *J. Virol.* **79**, 3139–3145.
  110. Liu, H. W., Cosa, G., Landes, C. F., Zeng, Y., Kovaleski, B. J., Mullen, D. G. *et al.* (2005). Single-molecule FRET studies of important intermediates in the nucleocapsid-protein-chaperoned minus-strand transfer step in HIV-1 reverse transcription. *Biophys. J.* **89**, 3470–3479.
  111. Zuker, M. (2003). Mfold web server for nucleic acid folding and hybridization prediction. *Nucleic Acids Res.* **31**, 3406–3415.